High rate gas dosing for tip based nanofabrication processes

M. P. Kanouff, J. N. Randall, M. Nadesalingham, W. P. Kirk, and R. M. Wallace

Citation: J. Vac. Sci. Technol. B **27**, 2769 (2009); doi: 10.1116/1.3259955
View online: http://dx.doi.org/10.1116/1.3259955
View Table of Contents: http://avspublications.org/resource/1/JVTBD9/v27/i6
Published by the AVS: Science & Technology of Materials, Interfaces, and Processing

Related Articles

Fabrication of hierarchical nanostructures using free-standing trilayer membrane
J. Vac. Sci. Technol. B 31, 06FF04 (2013)

Introduction to XPS Characterization of the Materials in Novel Carbon Nanotube-Based, Microfabricated, Thin Layer Chromatography Plates
Surf. Sci. Spectra 20, 35 (2013)

Growth of one-dimensional vertically aligned carbon nanostructures on SiC—Catalyst effect
J. Vac. Sci. Technol. A 31, 060603 (2013)

Fluorine-Doped Iron Oxide Nanomaterials by Plasma Enhanced-CVD: An XPS Study
Surf. Sci. Spectra 20, 9 (2013)

Synthesis, properties, and applications of silicon nanocrystals
J. Vac. Sci. Technol. B 31, 020801 (2013)

Additional information on J. Vac. Sci. Technol. B

Journal Homepage: http://avspublications.org/jvstb
Journal Information: http://avspublications.org/jvstb/about/about_the_journal
Top downloads: http://avspublications.org/jvstb/top_20_most_downloaded
Information for Authors: http://avspublications.org/jvstb/authors/information_for_contributors

ADVERTISEMENT

Downloaded 25 Sep 2013 to 129.110.33.9. Redistribution subject to AVS license or copyright; see http://avspublications.org/jvstb/about/rights_and_permissions

High rate gas dosing for tip based nanofabrication processes

M. P. Kanouff[a)]
Thermal/Fluid Science and Engineering, Sandia National Laboratories, Livermore, California 94550

J. N. Randall
Zyvex Labs, Richardson, Texas 75081

M. Nadesalingham, W. P. Kirk, and R. M. Wallace
Department of Materials Science and Engineering, University of Texas at Dallas, Richardson, Texas 75081

(Received 7 July 2009; accepted 15 October 2009; published 2 December 2009)

Tip based nanofabrication (TBN) processes promise unprecedented degrees of control and precision for the manufacture of nanostructured materials and devices. These processes use atomic force microscope or scanning tunneling microscope tips to create localized electric fields, electron beams, and other catalyzing conditions to control and detect the position, size, dimension, and orientation of nanostructures. Tip based approaches have deposited metals, oxides, and organic molecules to name a few. Often, a gas phase precursor is required to provide the material for the deposit. The TBN conditions for gas dosing are unique compared to other fabrication processes, e.g., chemical vapor deposition. The manufacture of precision nanostructures requires a contamination-free environment, and hence ultrahigh vacuum conditions must be maintained in the chamber. This can cause a gas jet from a doser to spread into a wide fan resulting in a small precursor flux with a broad distribution. This makes it difficult to meet the large fabrication rates desired for TBN. Ideally, gas dosing would promote rapid deposition rates while limiting the chamber pressure by creating a focused gas jet that is restricted to the intended fabrication area. Continuum gas dynamics and direct simulation Monte Carlo calculations were used to study the effect of design and operational parameters on gas doser performance. The source pressure, doser design, and operating conditions are shown to affect the flux distribution at the substrate. The calculated results are compared to experimental measurements. A novel gas doser design was identified and its performance predicted. © *2009 American Vacuum Society.* [DOI: 10.1116/1.3259955]

I. INTRODUCTION

Tip based nanofabrication (TBN) is a method for fabricating nanostructures (e.g., wires, dots, tubes) while controlling key characteristics such as their position, orientation, size, etc. A wide variety of methods are being considered including methods based on the use of scanning tunneling microscope (STM) tips to catalyze deposition of various species, initially supplied in the gas phase, onto a wafer substrate. Tip based approaches have deposited metals,[1] oxides,[2] and organic molecules[3] to name a few. This process is remotely similar to conventional chemical vapor deposition (CVD) processes used to create thin films in that the building material for the film starts out in the gas phase. However, in CVD a uniform deposition onto a wafer over a relatively large area is desired, while in TBN deposition is desired only over very small areas on the wafer. The high precision requirements for TBN mandate the use of ultraclean practices, including the preservation of very low pressures in the fabrication chamber even during the gas dosing procedure. Furthermore, the desire for a rapid fabrication process imposes the requirement for a large precursor deposition rate. The deposition rate depends on both the precursor flux and its sticking coefficient on the wafer. To achieve a large flux while limiting the chamber pressure, the gas dose must be focused and restricted to the intended deposition area. Sticking coefficients depend on the precursor, the surface conditions, wafer temperature, and impact kinetic energy of the precursor on the wafer.

Several designs for gas dosers have been discussed in the literature.[4–6] There are two extremes in terms of doser design, orifices where the doser diameter is large compared to its length, and capillaries where the length is large compared to the diameter of the doser. The performance of these two extremes depends on the Knudsen number Kn (gas mean free path divided by a doser length scale). The literature on gas doser design is primarily focused on cases where a uniform flux over a large portion of the wafer is desired, so arrays of orifices or capillaries are often considered that can produce good uniformity for small distances between the doser and wafer.

The precursor deposition rate can also be improved by increasing the sticking coefficient. For a given process, the sticking coefficient depends on the wafer temperature and impact kinetic energy. The choice of wafer temperature for TBN is somewhat limited. Large temperatures increase surface diffusion rates that can dismantle a nanodeposit, and low temperatures can lead to poor ordering of the deposited materials. Also, some TBN methods begin with a surface passivated with hydrogen, and then it is depassivated in small selected regions where nanostructures are to be deposited. High wafer temperatures can depassivate the surface in

[a)]Electronic mail: kanouff@sandia.gov

Downloaded 25 Sep 2013 to 129.110.33.9. Redistribution subject to AVS license or copyright; see http://avspublications.org/jvstb/about/rights_and_permissions

regions outside of the intended deposition location. Large impact kinetic energy can be obtained with supersonic nozzles, however, they require large source pressures to achieve large velocities that result in large flow rates and large chamber pressures. Other methods of obtaining large velocities are to heat the doser or to use a carrier gas. Heating the doser has merit and should be studied further. Using a carrier gas with small molecular weight relative to the precursor gas increases the velocity of the precursor, but at the expense of a larger total gas flow rate, which again leads to larger chamber pressures. A potential problem with large impact velocities of the precursor gas is that they might result in deposition on regions of the wafer that are passivated.

This article describes calculations carried out to study gas dosing methods in vacuum environments. The flux distributions of the precursor gas, disilane, on a wafer from various gas doser designs were calculated. Comparisons were made to flux distributions published in the literature. A novel design was identified for a gas doser that creates a focused flux with large magnitude at the intended target location for nanodeposits on the wafer.

II. BACKGROUND

When a gas flows from a region of large pressure to one of small pressure there is a conversion of thermal energy into kinetic energy where the mean gas velocity can reach very large values. This conversion process occurs through intermolecular collisions, and these collisions determine the flow path and thermodynamic behavior of the gas. A key parameter characterizing this behavior is the Knudsen number, which provides a measure of the number of collisions expected within the system length scale of interest. To characterize the flow from a gas doser in a vacuum environment a range of gas densities and system length scales must be considered. The flow internal to the doser may be characterized by a value of Kn based on the source gas density and doser diameter. External to the doser Kn should be based on the chamber pressure and distance between the doser and wafer. For conditions of interest here and a typical precursor of disilane, Kn values vary between 0.03 in the doser and 370 in the vacuum chamber. Approaches to modeling gas flows based on continuum theory, i.e., the Navier–Stokes equations, are generally considered valid only for $\mathrm{Kn} < 0.1$. Thus, an atomistic approach is required for the conditions of interest here.

Direct simulation Monte Carlo (DSMC) is an atomistic method of simulating rarefied gas flows.[7] It models the gas with a collection of computational particles, each representing a large number of real gas molecules. The particles are given initial positions and velocities, and there movement is calculated over a series of time steps. At the end of each time step the particles are sampled for collisions. A computational mesh is used to assist this collision sampling procedure, where only those particles located in the same mesh cell are considered for collision. Collision probabilities are calculated for each candidate pair of particles based on their collision cross sections and the ratio of real to computational particles. After the particles undergoing collisions have been identified they are given new velocities for the next time step. Thus, the DSMC method is deterministic for molecular trajectories and it is probabilistic for intermolecular collisions.

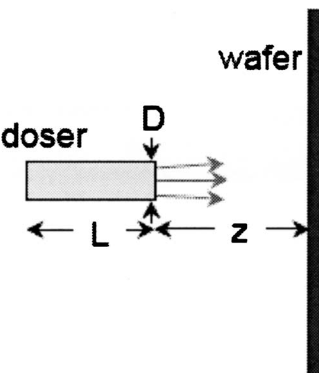

FIG. 1. Schematic of a tubular gas doser showing key dimensions.

III. MODEL DESCRIPTION

The basic geometry considered in this work is shown in Fig. 1. All of the DSMC calculations were carried out assuming axial symmetry. These results can be used to study the effects of off-normal angles between the doser and wafer through three-dimensional transformations. Such transformations are valid due to the free molecular nature of the flows, e.g., the lack of intermolecular collisions in the vicinity of the wafer means the molecules reflecting off the wafer do not influence the incoming molecular trajectories. The DSMC code, ICARUS,[8] was used to carry out all calculations.

The design of an individual tubular gas doser is defined by its length L and diameter D, as shown in the schematic in Fig. 1. Also important is its distance z from the wafer. Boundary conditions describing the source gas density, temperature, and properties are applied at the inlet to the doser. Perfect vacuum conditions are applied to the outer boundaries enclosing the computational domain, i.e., any computational particle crossing this boundary is permanently lost.

The precursor in the calculations carried out here was assumed to be disilane, Si_2H_6, with molecular size, $d = 0.6109 \times 10^{-7}$ cm, and mass, $m = 0.1033 \times 10^{-21}$ g. The computational particles were given three degrees of freedom for both rotational and translational motions, where five collisions were assumed to be required to equilibrate rotation with translation. The variable hard sphere model[7] was used where the collision cross section is dependent on the relative velocity between collision pairs. Surface collisions were assumed to be diffuse, where the angle of reflection is independent of the angle of incidence of a molecule on a surface.

An important nondimensional parameter is the source Knudsen number, $\mathrm{Kn}_0 = \lambda_0 / D$, where λ_0 is the mean free path in the "high" pressure source gas. Also important are the doser aspect ratio, L/D, where large values of this parameter describe a capillary and small values describe an orifice. The

Downloaded 25 Sep 2013 to 129.110.33.9. Redistribution subject to AVS license or copyright; see http://avspublications.org/jvstb/about/rights_and_permissions

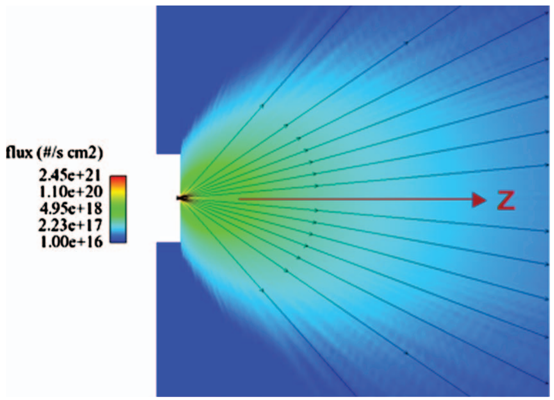

FIG. 2. (Color) Gas flux from a simple orifice-type doser (p_0=6.5 torr, Kn_0=0.028).

distance to diameter ratio, z/D, is also a key parameter where the doser appears as a point source when z/D is large.

IV. RESULTS

Figure 2 shows the molecular flux field from an orifice doser for typical conditions. The source pressure is 6.5 torr, and the orifice diameter is 100 μm (L=100 μm), resulting in Kn_0=0.028. The results show that the gas jet from this doser fans out in the vacuum environment. This behavior results in small flux magnitudes even at small distances from the doser where a wafer might be located.

The axial profiles of velocity and temperature are shown in Fig. 3. The gas velocity rapidly increases after exiting the orifice, and then comes to a constant value. Behavior similar to this is predicted by continuum theory, although the velocity predicted by continuum theory, 567 cm/s for the conditions considered here, is much larger than the result shown in Fig. 3(a) (~450 cm/s). This is due to the lack of intermolecular collisions that are assumed to take place in the continuum. It is well known that for large Kn_0 the maximum gas velocity that is attained will be less than the continuum result,[9] and the difference increases with Kn_0. The results for temperature show that the gas is not in equilibrium where the rotational and translational components of temperature are not the same. Continuum theory would predict that all temperature components would decrease monotonically with distance from the doser. The DSMC results show that rotational temperature is the first to depart from the continuum behavior, followed by the axial component of the translational temperature. Only the radial component of the translational temperature follows the continuum behavior. This departure from continuum behavior is due to the loss of intermolecular collisions a short distance from the doser. The mean free path of the gas (not shown) increases with distance from the doser to a value of 10 cm 5 mm from the doser.

The flux distribution on a wafer oriented perpendicularly to the gas jet axis is shown in Fig. 4. The results are rendered nondimensional by multiplying the flux by z^2 and dividing it by the total flow rate (molecule/time) from the doser and plotting it versus the radial distance on the wafer from the flux axis r divided by z. This scaling shows that results for dosers operating with $Kn_0 < 0.23$ [Fig. 4(a)] all collapse (approximately) to one curve for both orifice and capillary geometries, for a range of D values, for a range of flow rates, and for a range of z values. This is due to a large number of intermolecular collisions internal to the doser that dominate the behavior of the gas flow over that from surface collisions such that the geometry of the bounding walls of the doser is not important. In addition, although the results correspond to a range of z values, in all cases z is large compared to D such that the doser appears as a point source. This scaling clarifies the flux dependence on the design and operational parameters. The flux is directly proportional to the total flow rate, which is directly proportional to the source gas number density and the doser diameter squared. Also, the flux is inversely proportional to the distance z squared.

For comparison, results for an effusive emitter are included in Fig. 4(a), where both analytical and numerical solutions are presented. An effusive emitter is obtained with an orifice that has zero length, and by operating in the regime $Kn_0 \gg 1$, such that the flow is in the pure free molecular regime. Figure 4(a) shows that a doser operating with small Kn_0 provides a more focused flux than an effusive emitter, i.e., a flux that is larger for small values of r/z and smaller for large values of r/z. This appears to be due to the intermolecular collisions that take place for small Kn_0 internal to the doser that accelerate the gas in the axial direction more than in the radial direction. From this standpoint a small Knudsen number is preferred, but the Knudsen number rap-

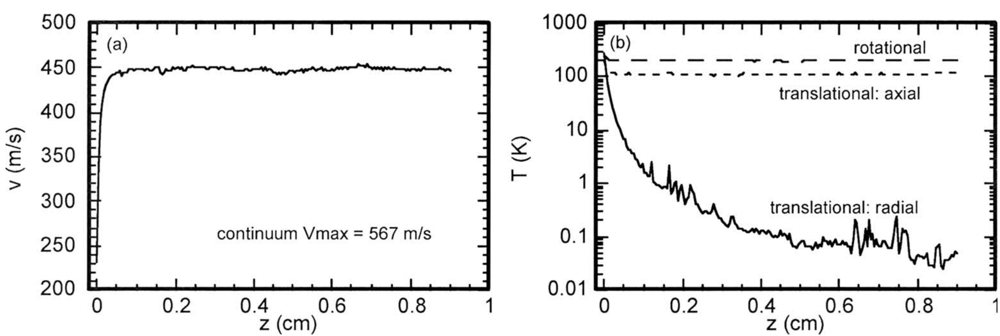

FIG. 3. Axial velocity (a) and temperature (b) profiles from a simple orifice-type doser (p_0=6.5 torr, Kn_0=0.028).

Downloaded 25 Sep 2013 to 129.110.33.9. Redistribution subject to AVS license or copyright; see http://avspublications.org/jvstb/about/rights_and_permissions

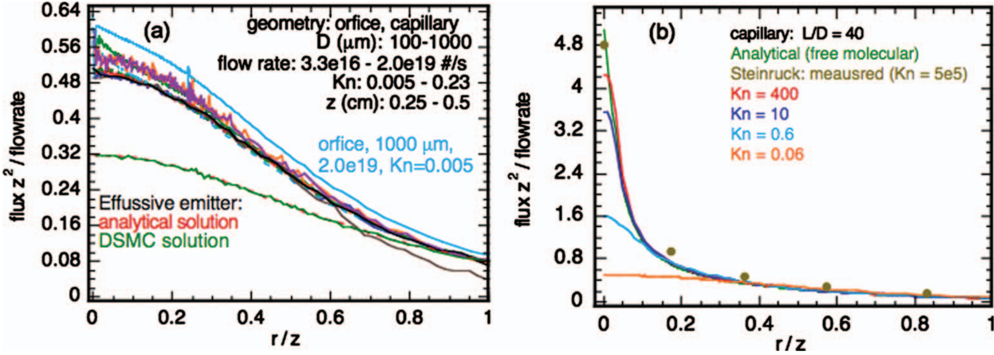

FIG. 4. (Color) Scaled flux distributions from (a) dosers operated at small Kn_0, where the curve colors indicate various combinations of design, D, flowrate, Kn_0, and z values (analytical and DSMC results for an effusive emitter also shown); (b) capillary-type dosers for a range of Kn_0 values.

idly increases with distance from the doser in the vacuum chamber. This limits the focusing effect to the modest levels seen in the figure.

Figure 4(b) shows the flux distribution from a capillary doser for a range of Kn_0. As Kn_0 increases the flux becomes increasingly focused. This is consistent with both an analytical solution for a capillary in free molecular flow and measurements by Steinruck[10] for a capillary operating at very large Kn_0. In this flow regime the capillary is acting as a filter that favors passage of those molecules moving parallel to its axis and rejects those molecules moving at an angle to the axis, with a high degree of probability. That is, a molecule moving at an angle to the axis of a long capillary will impact the capillary wall. After reflecting from the wall the molecule has a 50% probability of moving back toward the source side of the capillary, and those that continue to move in the forward direction are likely to suffer additional wall impacts, which at the very least will slow their average travel speed through the capillary such that they represent a small fraction of the total gas transmitted.

At this point a comparison can be made between the basic doser designs that have been discussed. Consider as a goal a fabrication rate of one nanodeposit per second per STM tip. Allowing for tip transit time there may only be one-half second available for the actual deposition process. Further assume that 5 ML must be deposited by the doser per nanodeposit. Then there is 0.1 s available to deposit 1 ML. A survey of the literature[11–14] shows a wide range of results for the dose required to deposit a monolayer on silicon using disilane as the precursor, as shown in Table I. Using a value near the middle of this range, 10^{17}, gives a requirement for the flux from the doser of $(10^{17}/0.1\ \text{s}=)10^{18}\ \#/\text{cm}^2\,\text{s}$. Finally, assume $z=0.5$ cm and the doser is perpendicular to the wafer. The different doser designs will be compared under these conditions. Here the peak values of the nondimensional fluxes shown in Fig. 4 are used, where a value for the total flow rate is selected that results in a wafer flux of 10^{18}.

A case with no doser is considered as a standard, where the fabrication chamber is simply filled with the precursor gas at a uniform chamber pressure (UCP). Under this condition the flux to the surface of a wafer is given by

$$\text{flux} = \frac{p\bar{v}}{4kT}, \quad \bar{v} = \sqrt{\frac{8kT}{\pi m}}, \tag{1}$$

where $\bar{v}$ is the mean molecular speed, p is the chamber pressure, T is the gas temperature (room value assumed), and k is Boltzmann's constant. A vacuum pump speed of 300 l/s is assumed for cases with dosers to calculate the chamber pressure resulting from the doser flow rate. The results of the comparison are shown in Table II. The standard (UCP) requires a chamber pressure of 3.9 mtorr to produce a flux of 10^{18}. An effusive doser requires a flow rate of 7.8×10^{17} resulting in a chamber pressure of 0.081 mtorr, just over 2% of that required by the standard. An orifice doser operating at small Kn_0 results in a chamber pressure just over 1% of that required by the standard. Moreover, a doser based on capillaries operating at large Kn_0 results in a chamber pressure less than 0.2% of that required by the standard. Thus, gas dosers can create a large flux without creating a large chamber pressure, and a doser based on capillaries is by far the best in this regard.

It should be noted that operating a capillary at large Kn_0 requires a small source gas density, which results in a small

TABLE I. Experimental results for the dose required to saturate a silicon surface using disilane.

Investigator	Wu[a]	Suda[b]	Gates[c]	Koulmann[d]
Dose ($\#/\text{cm}^2$)	1×10^{16}	8×10^{17}	1×10^{18}	3×10^{18}
Surface (Si)	[100]	[001]	[111]	[111]

[a]Reference 11.
[b]Reference 12.
[c]Reference 13.
[d]Reference 14.

TABLE II. Comparison of the flow rate required to give a flux of $10^{18}\ \#\,\text{s}/\text{cm}^2$ from various dosers and the resulting chamber pressure assuming a pump speed of 300 l/s.

	UCP	Effusive	Orifice	Capillary
Rate (#/s)	NA	7.8×10^{17}	4.6×10^{17}	5×10^{16}
p (mtorr)	3.9	0.081	0.048	0.0069
p/p_{UCP}	1	0.021	0.012	0.0018

Downloaded 25 Sep 2013 to 129.110.33.9. Redistribution subject to AVS license or copyright; see http://avspublications.org/jvstb/about/rights_and_permissions

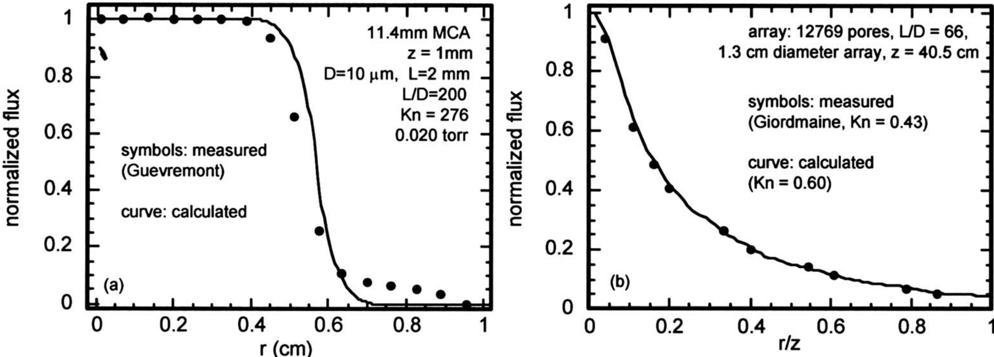

FIG. 5. Gas flux distributions from microcapillary arrays for small (a) and large (b) distance to diameter ratios.

flow rate. So while the flux from a capillary is very focused for large Kn_0, it is also very small, i.e., the nondimensional results in Fig. 4(b) are converted to dimensional results by multiplying by the flow rate (and dividing by z^2). Consequently, for a capillary-type doser to provide a large flux, a large number of capillaries must be used. A technology that would be useful for this purpose is the microcapillary array (MCA), also called a microchannel plate.[15] It is made by fusing together a large number of glass capillaries, followed by drawing and cutting processes. The result is a plate composed of a large number of closely packed cylindrical pores with parallel axes. Typical dimensions are a pore diameter of 10 μm with 12 μm center-to-center spacing and a pore length of 400 μm, which gives an aspect ratio of $L/D=40$. A 1 mm diameter plate can have nearly 7000 pores.

Microcapillary arrays have been used in prior gas doser designs[4–6,16–22] where the objective was to create a uniform flux over a large portion of a crystal surface. The DSMC results for a single capillary can be superimposed to obtain the combined flux distribution from an array where account is taken for the number of pores and their layout pattern in the array. This superposition is valid due to the lack of intermolecular collisions in the large Kn_0 regime, such that the gas plumes emitted by the individual pores do not interact. Superimposed results are shown in Fig. 5 using the conditions of Guevremont[6] [Fig. 5(a)] and Giordmaine[23] [Fig. 5(b)]. The flux distribution in Fig. 5(a) is for a case where the distribution is along a radial line relatively close to the array (z/array diameter=0.09) and that in Fig. 5(b) is for a flux distribution far from the array (z/array diameter=31). As can be seen, the central section of the distribution is uniform for small z/D while the distribution has a more focused appearance for large z/D. The agreement between measured and calculated results is good in both cases.

The TBN application calls for a different design for the microchannel plate, as shown schematically in Fig. 6(a). A curved plate such that the axes of all the pores intersect at a focal point would be ideal. Several of these could be combined in a single doser design to provide the needed total flow rate where each plate is aimed at the target, as shown in Fig. 6(b). This figure illustrates how the MCAs could be arranged around other hardware that might be present, such as a STM tip. Note that curved microchannel plates have been fabricated, where they were used in molecular beam studies by Ma.[24]

Conventional flat microchannel plates could also be used in a design similar to that shown in Fig. 6(b). It should be noted, however, that the flux from a flat microchannel plate is not as focused as that from a single capillary (or that from a curved microchannel plate), even for large z/D, as shown in Fig. 7 for a plate of 1 mm in diameter and for $z/D=5$. It still has merit though since the flux distribution from the small flat array is more focused than that from an orifice operating at small Kn_0 or that from an effusive emitter.

As an example, the flux field from a ring of capillaries encircling a probe and aimed at the deposition target area on a wafer is shown in Fig. 8. By approaching the target from 45° angles and distributing the capillaries (or microchannel

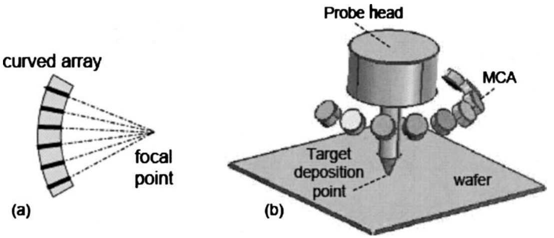

FIG. 6. Features of advanced gas doser designs; (a) a curved MCA that focuses the flux from many capillaries and (b) an arrangement of nine small MCAs individually aimed at the target.

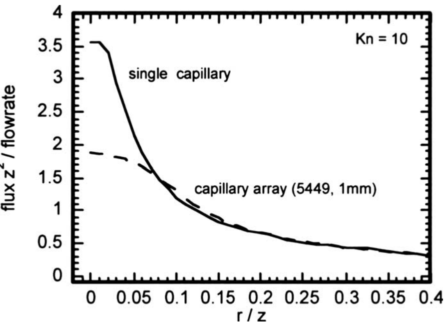

FIG. 7. Scaled gas flux from a single capillary compared to that from a small MCA ($z/D=5$, $p_0=0.19$ torr, $Kn_0=10$).

Downloaded 25 Sep 2013 to 129.110.33.9. Redistribution subject to AVS license or copyright; see http://avspublications.org/jvstb/about/rights_and_permissions

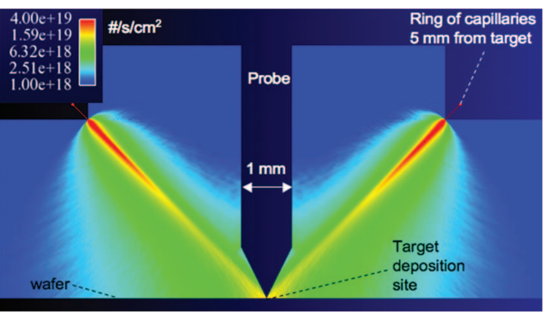

FIG. 8. (Color) Gas flux distribution from a focused capillary-type doser (p_0=0.005 torr, Kn_0=400).

plates) around the probe the capillary-based design should be able to accommodate any access constraints that are likely to exist in TBN processes.

Detailed flux distributions on the wafer surface are shown in Fig. 9 for three different doser designs. In all cases the dosers are 5 mm from the target location on the wafer, and the doser axis is at a 45° angle to the wafer normal, as shown in Fig. 9(a). Also, the total flow rates from the dosers are chosen such that the flux on the wafer at the target location ($x=y=0$) is 10^{18} #s/cm^2. The results presented here are based on axisymmetric DSMC calculations, where a three-dimensional transformation was applied to account for the off-normal angle of incidence. Figure 9(b) shows the distribution from an orifice doser design operating at small Kn_0. The maximum flux is not at the target location and it is far greater than 10^{18}. This is due to the wide spread distribution of gas that is emitted by this doser such that a lot of the gas impacts the wafer at points closer to the doser. This maximum flux occurs at a point that is not only closer to the doser than the target is but also where there is a more normal angle of incidence. Thus, most of the gas impacts the wafer at points other than the intended target, where this gas does not support the intended deposition and nanofabrication, but it does place additional burden on the vacuum pump.

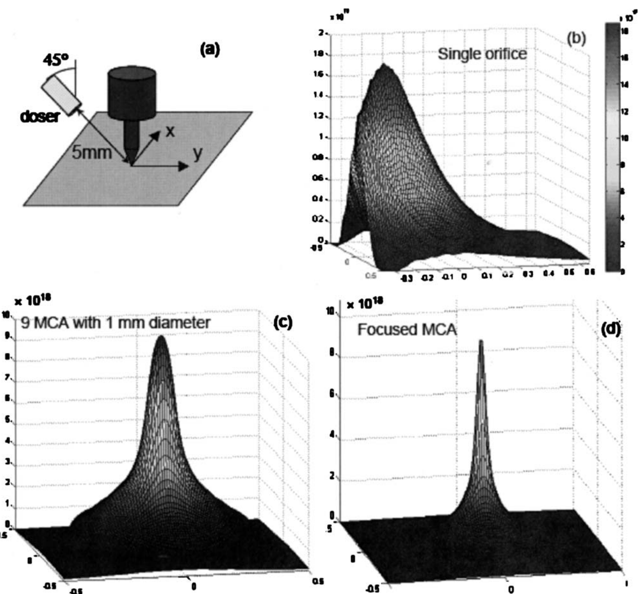

FIG. 9. Gas flux distributions over a 1 cm^2 wafer area from various gas dosers with (a) 45° approach angle and 5 mm distance access constraints; (b) an orifice doser with Kn_0=0.028, (c) nine flat MCAs with Kn_0=10, a focused MCA with 26523 capillaries, and Kn_0=10.

Figure 9(c) shows the flux distribution from nine 1 mm diameter flat microchannel plates. This distribution is far more efficient than that in Fig. 9(b) in terms of placing the flux at the target. Even more efficient is the distribution shown in Fig. 9(d), which results from a capillary-based design where all of the capillaries are aimed at the target, such as that which would occur if curved microchannel plates were used.

Note that the disilane dose required to deposit a monolayer on silicon is uncertain. For example, based on our preliminary experimental results a dose of 10^{16} may be sufficient to deposit a monolayer. Assuming 0.1 s is available for the dosing process, the required flux is only 10^{17} and the number of capillaries needed to create this flux is 2652, which is easily obtained with microcapillary arrays.

As a final discussion point, the results shown in Figs. 8, 9(c), and 9(d) are based on a design where the gas doser is placed in an arrangement around the STM tip at a radial distance of 3.5 mm (in the wafer plane). Although this separation distance was chosen somewhat arbitrarily, this general design will impose some constraints on how small the spacing may be between tip/doser assemblies in a process employing multiple tips for parallel fabrication. That is, the doser design described here may require that each tip has its own doser. The spacing between multiple tips will eventually have to be addressed, and while the program addressed here does call for a 30 tip array in its latter stages, it does not place a restriction on the tip-to-tip spacing. The intent is to first determine the details of the process that lead to rapid fabrication of a small number of deposits, including the gas dosing requirements and the STM tip hardware geometry. As discussed above, this may show that the gas dose required is much smaller than 10^{18} #s/cm^2, in which case a smaller number of capillary arrays would suffice that would permit a more compact doser design and closer spacing of multiple tip/doser assemblies. In the event that a large gas dose is required, the learning experience provided by starting with the doser design described here may lead to ideas about how to better arrange the capillary arrays that would allow for smaller tip-to-tip spacing.

V. CONCLUSIONS

Gas dosing for tip-based nanofabrication has requirements different than that in conventional chemical vapor deposition. Instead of a uniform flux over a large region of a wafer and a loose requirement on the fabrication rate, a large flux over a small region is needed that helps to meet a fast fabrication requirement. This is challenging due to the large dose required to deposit a monolayer, the multiple monolayers required to fabricate a nanodeposit, and the strong tendency for a gas jet or plume emitted by a doser to fan out. A wide spread jet results in a flux on the wafer that is small at all

Downloaded 25 Sep 2013 to 129.110.33.9. Redistribution subject to AVS license or copyright; see http://avspublications.org/jvstb/about/rights_and_permissions

points, and that portion of the emitted gas not directed at the target point serves no useful purpose, but it is detrimental to the process because it results in elevated chamber pressures that contribute to contamination of the nanodeposits. Focused gas jets can be obtained through the use of doser designs based on capillaries, but they require the use of small source gas pressures that result in small flow rates and small fluxes from single capillaries. A novel design was identified here that uses a large number of capillaries to obtain a large total flow rate, where the capillaries are all aimed at the target deposition point to obtain a large flux. This doser design can be realized through the use of curved microchannel plates or through the use of several small flat microchannel plates. Direct simulation Monte Carlo calculations were used to confirm the superior performance of this doser design over that of other designs.

ACKNOWLEDGMENTS

This research was funded by the DARPA Micro Technology Office. Sandia is a multiprogram laboratory operated by Sandia Corporation, a Lockheed Martin Company, for the United States Department of Energy contract/Grant No. DEAC04-94-AL85000.

[1]D. P. Adams, T. M. Mayer, and B. S. Swartzentruber, Appl. Phys. Lett. **68**, 2210 (1996).
[2]P. Fay, R. T. Brockenbrough, G. Abeln, P. Scott, S. Agatwala, I. Adesida, and J. W. Lyding, J. Appl. Phys. **75**, 7545 (1994).
[3]G. C. Abeln, M. C. Hersam, D. S. Thompson, S.-T. Hwang, H. Choi, J. S. Moore, and J. W. Lyding, J. Vac. Sci. Technol. B **16**, 3874 (1998).
[4]C. T. Campbell and S. M. Valone, J. Vac. Sci. Technol. A **3**, 408 (1985).
[5]D. E. Kuhl and R. G. Tobin, Rev. Sci. Instrum. **66**, 3016 (1995).
[6]J. M. Guevremont, S. Sheldon, and F. Zaera, Rev. Sci. Instrum. **71**, 3869 (2000).
[7]G. A. Bird, *Molecular Gas Dynamics and the Direct Simulation of Gas Flows* (Clarendon, Oxford, 1994).
[8]T. J. Bartel, S. Plimpton, and M. A. Gallis, Sandia National Laboratories Report No. SAND2001-2901, 2001.
[9]G. Scoles, *Atomic and Molecular Beam Methods* (Oxford University Press, New York, 1988), pp. 25–38.
[10]H. P. Steinruck and K. D. Rendulic, Vacuum **36**, 213 (1986).
[11]Y. M. Wu and R. M. Nix, Surf. Sci. **306**, 59 (1994).
[12]Y. Suda, J. Vac. Sci. Technol. A **15**, 2463 (1997).
[13]M. Gates, Surf. Sci. **195**, 307 (1988).
[14]J. J. Koulmann, F. Ringeisen, M. Alaoui, and D. Bolmont, Phys. Rev. B **41**, 3878 (1990).
[15]BURLE Industries, Inc., http://www.burle.com/detectors.htm
[16]A. Winkler and J. T. Yates, J. Vac. Sci. Technol. A **6**, 2929 (1988).
[17]R. H. Jones, D. R. Olander, and V. R. Kruger, J. Appl. Phys. **40**, 4641 (1969).
[18]D. R. Olander, J. Appl. Phys. **40**, 4650 (1969).
[19]D. R. Olander, and V. R. Kruger, J. Appl. Phys. **41**, 2769 (1970).
[20]D. R. Olander, R. H. Jones, and W. J. Siekhaus, J. Appl. Phys. **41**, 4388 (1970).
[21]W. J. Siekhaus, R. H. Jones, and D. R. Olander, J. Appl. Phys. **41**, 4392 (1970).
[22]D. M. Murphy, J. Vac. Sci. Technol. A **7**, 3075 (1989).
[23]J. A. Giormaine and T. C. Wang, J. Appl. Phys. **31**, 463 (1960).
[24]Y. Ma, B. Y. H. Liu, and H. S. Lee, J. Vac. Sci. Technol. A **14**, 2414 (1996).

Downloaded 25 Sep 2013 to 129.110.33.9. Redistribution subject to AVS license or copyright; see http://avspublications.org/jvstb/about/rights_and_permissions